Pressure and Temperature Control of Spin-Switchable Metal-Organic Coordination Polymers from *Ab Initio* Calculations

K. Tarafder,[1] S. Kanungo,[2] P. M. Oppeneer,[1] and T. Saha-Dasgupta[2]

[1]*Department of Physics and Astronomy, Uppsala University, P. O. Box 516, SE-751 20 Uppsala, Sweden*

[2]*S. N. Bose National Centre for Basic Sciences, Kolkata 700098, India*

(Received 15 April 2012; published 16 August 2012)

We explore a combination of density-functional theory with supplemented Coulomb U (DFT + U) and *ab initio* molecular dynamics simulations to investigate the spin-crossover (SCO) phenomenon in coordination polymers. We demonstrate the applicability of the method for the case of bimetallic metal-organic framework $Fe_2[Nb(CN)_8] \cdot (4\text{-pyridinealdoxime})_8 \cdot 2H_2O$ [see S. Ohkoshi *et al.* Nat. Chem. **3**, 564 (2011)]. Our study shows that this approach is capable of capturing the SCO transitions driven by pressure as well as temperature. In addition to discovering novel spin-state transitions, magnetic states involving changes in the long-range magnetic ordering pattern are achieved, thereby offering the tunability of spin states as well as the long-range order of the spins. We compare the SCO transition in the Fe-based framework with a computer designed Mn-based variant.

DOI: 10.1103/PhysRevLett.109.077203 PACS numbers: 75.30.Wx, 71.15.Mb, 71.20.Be

Introduction.—Spin-crossover (SCO) transition is a phenomenon that can occur in octahedrally coordinated transition-metal ions of d^4-d^7 configuration in which the spin state switches reversibly between different values due to an external perturbation such as pressure, temperature, light irradiation, or magnetic field [1]. Such SCO transitions on Fe have been observed in Fe-bearing silicate perovskite under lower mantle pressure in Earth's interior [2]. They have been observed, too, for coordination polymers [3] with Fe^{2+} building blocks [4], which hold promise for construction of advanced materials with various applications, such as spin-switchable memory devices, optical information storage and displays [5]. Through communication between individual SCO centers cooperativity builds up, thereby providing a bistable character to the whole material. In spite of its technological importance, the SCO phenomenon in coordination polymers is not yet well understood, especially on the materials level.

While the SCO transition can be qualitatively understood, following ligand field theory [6], as a competition between the splitting between t_{2g} and e_g energy levels, and the Hund's rule coupling (J_H) between the d electrons, it does not offer a predictive, materials specific explanation of the phenomenon. Most importantly, it does not take into account the building up of long-range order in the extended framework. Theoretical works to address cooperativity in SCO materials are based on elastic interactions, defined in terms of local distortions interacting elastically and producing long-range effective interactions [7]. Only recently the possible role of magnetic exchange in cooperativity has been investigated [8]. A viable route to microscopic understanding of the SCO phenomenon and its cooperativity in extended systems like coordination polymers would be to employ density-functional theory (DFT) based calculations. This is however very challenging given the complex nature of the crystalline environment involving several SCO atoms in the unit cell and, moreover, the description of the phenomenon requires proper handling of the subtle changes in the crystal structure as well as the electronic structure upon application of external stimuli. Nonetheless, with the advancement of *ab initio* techniques in terms of accounting for the open-shell correlation effect, which is important for capturing correctly the transition-metal d electrons, the established confidence in accurately predicting the changes in crystal structures in such metal-organic polymers [9,10] is growing. Also, the capability of handling temperature effects through *ab initio* molecular dynamics (AIMD) simulations is promising [11].

In this Letter, we explore a combined structural-temperature approach to the SCO phenomenon considering the example of a recently synthesized bimetallic, coordination polymeric compound, $Fe_2[Nb(CN)_8] \cdot (4\text{-pyridinealdoxime})_8 \cdot 2H_2O$ [12]. Using a combination of *ab initio* DFT + U and AIMD, we study the effects of application of hydrostatic pressure, temperature, as well as of substitution of Fe^{2+} by Mn^{2+}. We could successfully describe the pressure as well as temperature-driven spin-state transition, establishing thus the potential of the introduced approach in adequately handling such complex phenomenon. In the combined pressure-temperature route, we predict the existence of two interesting, as yet undiscovered phases. One of these has the intermediate spin (IS) state of Fe^{2+} as opposed to the high-spin (HS) or low-spin (LS) state. Interestingly, this IS state exhibits long-range ferromagnetic coupling between the Fe and Nb spins, as opposed to long-range antiferromagnetic coupling between the HS Fe and Nb spins observed experimentally at ambient pressure [12]. With temperature, this ferromagnetic coupled IS state can be switched to a different HS state, with ferromagnetic coupling between HS Fe and Nb spins.

Through the pressure and temperature control, our study thus predicts switching of the Fe-spin state together with switching of the long-range magnetic order. Substitution of Fe by Mn leads to changes in the nature of pressure driven spin-state transition from a two-step (HS → IS → LS) to a one-step (HS → LS) process.

Method.—The DFT calculations, reported in this study, were carried out using the plane wave, pseudopotential basis as implemented in Vienna *ab initio* simulation package (VASP) package [13] with choice of projector-augmented wave (PAW) potential [14]. The exchange-correlation functional was chosen to be the generalized gradient approximation (GGA) [15]. The missing correlation effect beyond GGA was accounted for through DFT + U [16] calculations. This approach has given promising results for SCO systems [9,17]. The AIMD calculations in this work were performed using VASP in the NVT ensemble, where N is the number of particles, V is the volume of each system, and T is the temperature of the ensemble. Details of the computations can be found in the Supplemental Material [18].

The system.—$Fe_2[Nb(CN)_8]\cdot(4\text{-pyridinealdoxime})_8\cdot 2H_2O$ forms a three-dimensional connected network of cyanide (CN)-bridged Fe–Nb atoms, which crystallizes in the tetragonal space group $I4_1/a$ [12]. The basic structural units consist of distorted FeN_6 octahedra and NbC_8 dodecahedra. The octahedral and dodecahedral units are connected to each other through C–N bridges, as shown in the inset of Fig. 1. The two apical positions of the octahedral units are formed by cyanide N atoms while the other four positions are formed by N atoms belonging to rings of 4-pyridinealdoxime. Among the eight CN groups connected to Nb, four are connected to Fe while the remaining four are free and saturated by hydrogens. Some of the waters are connected to the hydroxyl group of 4-pyridinealdoxime through hydrogen bridges and the rest are nonbonded, giving rise to a total of 290 atoms in the unit cell [19].

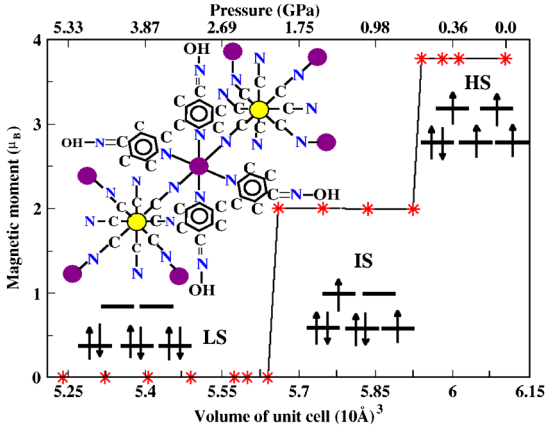

FIG. 1 (color online). Computed magnetic moment at the Fe site plotted vs the unit-cell volume of the Fe–Nb complex. The hydrostatic pressures corresponding to selected volumes are marked in the upper ordinate. The t_{2g} and e_g orbital occupations of Fe in HS, IS, and LS states are shown schematically. The inset shows the crystal structure, highlighting the environment around Fe, represented as magenta (dark) balls and Nb, represented as yellow (light) balls.

Structural optimization and volume-reduction effect.—The published crystal structure data [12] measured at 300 K do not report the positions of hydrogens which are difficult to detect through x-ray diffraction. In the first step, starting from the reported crystal structure data, we therefore positioned the hydrogen atoms at their suitable positions and relaxed their positions by minimizing the forces while keeping the positions of other atoms and the lattice constants fixed at their measured values. The computed electronic structure carried out on this structure shows the HS state of Fe with a magnetic moment (M^{Fe}) of $3.75\mu_B$. The moment at Nb site (M^{Nb}) is obtained to be $-0.58\mu_B$, aligned antiparallely to the Fe moment, establishing thus Fe^{2+} valence with $S = 2$ and Nb^{4+} valence with $S = 1/2$ spin and the antiferromagnetic coupling between Fe and Nb spins, as deduced in the experimental study [12]. In the next step, starting from the HS structure, we reduced the unit-cell volume keeping the aspect ratios the same as that of the HS structure, thereby emulating the application of hydrostatic pressure, and reoptimized all the atomic positions. The obtained results are summarized in the main panel of Fig. 1. Upon volume reduction, we find a remarkable, two-step spin transition process at the Fe site, with first transition from HS ($M^{Fe} = 3.75\mu_B$) to IS ($M^{Fe} = 2.00\mu_B$) upon volume reduction by $\approx 3\%$, and consecutively to LS ($M^{Fe} = 0.0\mu_B$) upon further reduction of volume by $\approx 7\%$, while the Nb moment stays more or less constant, $M^{Nb} \approx 0.6\mu_B$. This two-step transition is triggered by the changes in the Fe–N bond lengths (cf. [20]): the average Fe–N bond length along CN bridges reduces from a value of 2.04 Å at HS state to 1.93 Å at IS state to 1.91 Å at LS state. The average Fe–N bond length along the 4-pyridinealdoxime rings also shows a substantial change from an average value of 2.23 Å at HS state to 2.09 Å at IS state to 2.04 Å at LS state. We find the transitions to be extremely sharp, showing the cooperative nature (see Supplemental Material [18] for details). Considering bulk modulus values typical of metal-organic systems, $B_0 = 20$ GPa and $(\frac{\delta B_0}{\delta P})_{V_0} = 7$ [21], the volume reduction of $\approx 3\%$ (required to drive the HS → IS transition) would amount to application of about 1 GPa pressure while $\approx 7\%$ volume reduction (required to drive the HS → LS transition) would amount to about 2 GPa pressure. We note that the IS state of Fe^{2+}, though less common compared to LS or HS, has been reported in the literature [2].

The spin-polarized density of states (DOS) projected on Fe d, Nb d, C p, and N p are shown in Fig. 2, for HS, IS, and LS configurations. The top panel exemplifies the antiparallel alignment of HS Fe and Nb at ambient pressure.

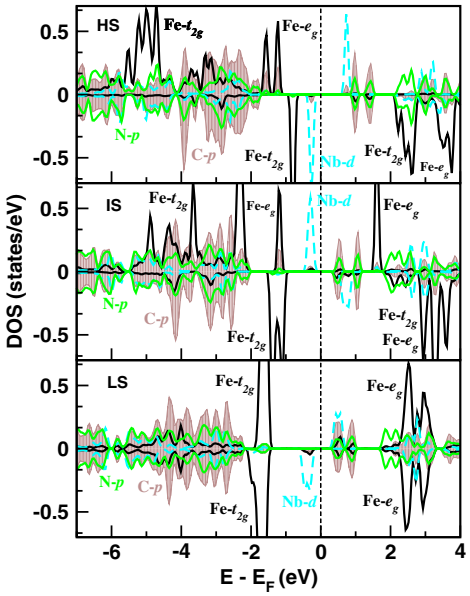

FIG. 2 (color online). Density of states projected onto spin-polarized Fe d (black, solid), Nb d (cyan, dashed), N p (green, solid), and C p (shaded area) states, for HS, IS, and LS configurations (top to bottom panel) of the Fe–Nb SCO compound. The zero energy is set at the Fermi energy (E_F). The upper and lower subpanels in each panel correspond to up and down spin channels, respectively.

Interestingly, we note that for the IS configuration, the relative alignment of Nb majority and minority spin states to that of Fe is reversed compared to that in HS state, i.e., predicting a parallel alignment of Fe and Nb spins. Note that within the DFT + U formulation, this metal-organic compound is predicted to be an insulator in the studied volume range.

Temperature effect and AIMD results.—Following the study of the effect of isotropic volume reduction (hydrostatic pressure), we focus on the effect of temperature. For this purpose, we carried out AIMD simulations, where the final temperatures were fixed at different values. First, starting from the ambient pressure 300 K HS state we could through AIMD simulations obtain the SCO transition to the LS state by fixing the quenching temperature to 20 K, in agreement with experimental observation [12]. The relative free energy difference between the HS and LS systems, $\frac{F^{\mathrm{HS}}-F^{\mathrm{LS}}}{F^{\mathrm{HS}}}$, is about 10^{-5}, and $\Delta F^{\mathrm{HS}\rightarrow\mathrm{LS}} =$ 25 kJ/mol, which agrees reasonably well with relative energy estimates for SCO molecular systems [22]. Second, starting from the $T = 0$ K optimized crystal structure of the IS state reported above, we carried out AIMD simulations setting the final temperature to 300 K. We found the AIMD simulation to predict a temperature-driven IS → HS transition. The AIMD simulation is thus capable of capturing the necessary expansion of the Fe–N bond lengths, from average value of 2.09 Å (1.93 Å) in the $T = 0$ K structure to 2.22 Å (2.05 Å) in the 300 K structure for the Fe-N bond lengths belonging to 4-pyridinealdoxime ring (CN bridges). The evolution of the average Fe–N bond length in the AIMD simulation is presented in the Supplemental Material [18]. The computed Fe magnetic moment of the 300 K crystal structure was found to be $3.73\mu_B$ in agreement with a HS state of Fe. This HS state (referred as HS-2 hereafter) however is *distinct* from the ambient pressure 300 K HS state (referred as HS-1 hereafter) in terms of the long-range magnetic order which consists of ferromagnetically aligned Fe and Nb spins with a total magnetic moment of $9.0\mu_B$/formula units, as opposed to the antiparallel aligned configuration HS-1 at ambient pressure 300 K, with a total magnetic moment of $7.0\mu_B$/formula units.

To understand the origin of this change of the nature of the magnetic coupling between Fe and Nb in the two different HS states, we plotted the magnetization density for the HS-1 and HS-2 state in Fig. 3. We observe that the magnetic interaction connecting Fe and Nb proceeds through the Fe–N–C–Nb super-superexchange path. Interesting changes happen with the bond angles in the connected path. While the Fe–N–C bond angle shows a change as large as about 8° between the HS-1 and HS-2 structures, the N–C–Nb bond angle shows little change. This modification causes the relative orientation of the magnetization density at Fe and N sites to flip from antiparallel in HS-1 to parallel in HS-2 (note the change in color of the density at N site). This in turn causes the sign of the magnetization densities at C and Nb sites to flip also, which are aligned antiparallely and parallely in HS-1 and

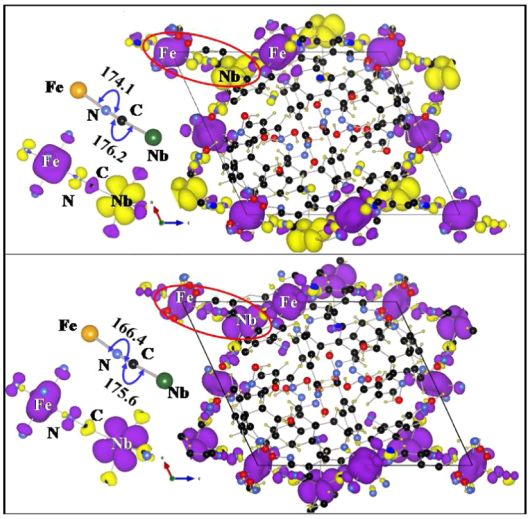

FIG. 3 (color online). Magnetization density plots for the HS-1 (upper panel) and HS-2 (lower panel) states (isosurface value set at 0.025/Å^3). The magenta (dark) and yellow (light) color indicates positive and negative values of the magnetization densities, respectively. Also shown are the structural comparison of the Fe–N–C–Nb path in HS-1 and HS-2, together with a zoomed plot of the magnetization density along the superexchange path.

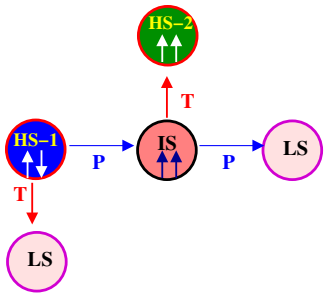

FIG. 4 (color online). Schematic representation of the temperature-pressure-induced spin-state transitions in the Fe–Nb framework.

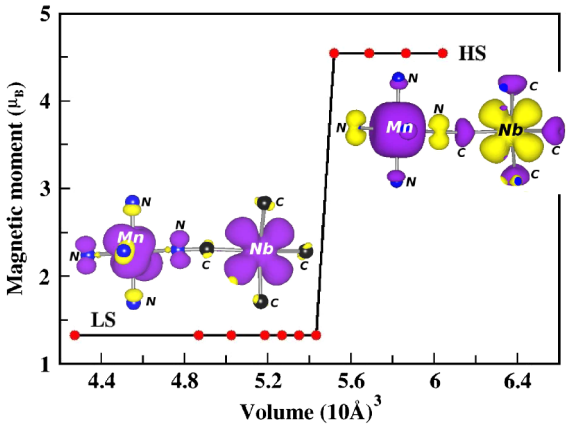

FIG. 5 (color online). Magnetic moment at the Mn site plotted against the unit-cell volume of the Mn–Nb complex. The magnetization density plots in the insets illustrate the pressure-induced switching from ferrimagnetic alignment between Mn^{2+} ($S = 5/2$) and Nb^{4+} ($S = 1/2$) to ferromagnetic alignment between Mn^{2+} ($S = 1/2$) and Nb^{4+} ($S = 1/2$) along the superexchange path.

HS-2 states, respectively, to the magnetization density at the N site. This change is reflected also in the calculated magnetic moments at N and C sites, which are found to be $-0.03\mu_B$ and $+0.03\mu_B$, respectively, for HS-1 and $+0.06\mu_B$ and $-0.01\mu_B$, respectively, for HS-2. The change in bond angle causes a change in hopping interactions and, importantly, change in the relative energy level positions, leading to changes in Fe–N hybridization between majority and minority spin channels, thereby flipping the sign of the induced moment at the N site.

The obtained pressure- and temperature-driven SCO transitions are summarized in the schematic diagram, Fig. 4, which forms the central point of our study. Note that only the temperature-induced transition between LS and HS-1 was thus-far observed [12]; all other states are *ab initio* predictions. The plot emphasizes that, employing the combined pressure-temperature route, complex evolution of various spin states can be uncovered and even the long-range order of spins can be tuned, opening up the possibility of designing SCOs from an antiferro- or ferrimagnet to a ferromagnet. A further interesting aspect of the SCO in coordination polymers is the existence of the thermal hysteresis loop. To assess the feasibility of our method to capture the thermal hysteresis, one would need to carry out AIMD simulations at many different temperature values with small intervals (the width of the hysteresis is estimated to about a few K [12]) which, for the current system with ~300 atoms in the unit cell, the existing computational resources did not allow us to do.

Mn substitution.—Lastly, we studied the influence of substitution of Fe by Mn. This was motivated by the fact that a Mn-based variant was also reported to be synthesized, though of somewhat different H_2O composition [12]. To study computationally the effect of Fe–Mn substitution, we started with experimental crystal structure data of the Fe–Nb compound measured at 300 K, replaced Fe by Mn, performed the full optimization of the crystal structure, unit-cell volume, as well as atomic positions. A HS state consisting of a Mn $S = 5/2$ spin aligned antiparallel to a Nb $S = 1/2$ spin was obtained, concordant with experimental observation [12] made on a related Mn–Nb framework. Subsequently, the effect of hydrostatic pressure was investigated. Upon volume reduction, a one-step transition from HS ($S = 5/2$) to LS state ($S = 1/2$) at the Mn site was achieved around a volume reduction of 10%, amounting to application of hydrostatic pressure of about 3 GPa (see Fig. 5). Comparing with Fe–Nb, we note: (a) the Mn variant exhibits one-step transition in contrast to the two-step transition predicted for the Fe compound; (b) the HS → LS transition requires a larger volume compression compared to that of the Fe compound. The latter is consistent with the larger HS moment of Mn compared to Fe, as well as the stronger Mn–Nb magnetic interaction (J) compared to Fe–Nb magnetic interaction (*ab initio* estimated $J_{\text{Mn-Nb}} = 5$ meV vs $J_{\text{Fe-Nb}} = 2$ meV) giving rise to a higher magnetic energy to be overcome in order to drive the HS → LS transition. Interestingly, we again obtained the change in the nature of the long-range magnetic order from a HS state with ferrimagnetic order of Mn–5/2 and Nb–1/2 spins to a LS state with ferromagnetic order of Mn–5/2 and Nb–1/2 spins.

In conclusion, using DFT + U and AIMD calculations offers a promising first-principles approach to SCO transitions. Through the combination of both pressure and temperature, not only the known LS → HS-1 switching of spin states of Fe in an Fe–Nb based bimetallic metal-organic coordination polymer could be explained, also switching to previously unknown spin states is unveiled. Moreover, our *ab initio* simulations predict switching of the long-range magnetic order, between ferri- and ferromagnetic. The pressures predicted to induce these switchings are in the range of 1–2 GPa, making verification in the laboratory feasible. Substitution of Fe by Mn leads to a one-step SCO transition between a Mn HS and LS state, as opposed to a two-step SCO transition obtained for the Fe–Nb coordination complex, from HS to IS and to LS.

The successful descriptions of the SCO transitions underline that *ab initio* calculations could in the near future be employed to map out the pressure-temperature phase diagram of SCO coordination complexes and even to design suitable SCO properties.

This work has been supported through the Swedish-Indian Research Links Program and Swedish National Infrastructure for Computing (SNIC). We thank Pablo Maldonado for valuable discussions.

[1] *Spin Crossover in Transition Metal Compounds*, Topics in Current Chemistry, edited by P. Gütlich and H. A. Goodwin, Vol. 233–235 (Springer, New York, 2004); V. Niel, A. L. Thompson, M. C. Muñoz, A. Galet, A. E. Goeta, and J. A. Real, Angew. Chem., Int. Ed. Engl. **42**, 3760 (2003); N. O. Moussa, G. Molnár, S. Bonhommeau, A. Zwick, S. Mouri, K. Tanaka, J. A. Real, and A. Bousseksou, Phys. Rev. Lett. **94**, 107205 (2005).

[2] See, for example, V. V. Struzhkin, H.-k. Mao, J. Shu, R. J. Hemley, Y. Fei, B. Mysen, P. Dera, V. Prakapenka, and G. Shen, Proc. Natl. Acad. Sci. U.S.A. **101**, 14027 (2004); C. McCammon, I. Kantor, O. Narygina, J. Rouquette, U. Ponkratz, I. Sergueev, M. Mezouar, V. Prakapenka, and L. Dubrovinsky, Nature Geosci. **1**, 684 (2008).

[3] O. Kahn and C. J. Martinez, Science **279**, 44 (1998).

[4] P. Gamez, J. Sánchez Costa, M. Quesada, and G. Aromí, Dalton Trans. 7845 (2009).

[5] See, for example, S. Bonhommeau, G. Molnár, A. Galet, A. Zwick, J. A. Real, J. J. McGarvey, and A. Bousseksou, Angew. Chem., Int. Ed. Engl. **44**, 4069 (2005).

[6] F. A. Cotton, G. Wilkinson, and P. L. Gaus, *Basic Inorganic Chemistry* (Wiley, New York, 1995), 3rd ed.

[7] P. Gütlich, A. Hauser, and H. Spiering, Angew. Chem., Int. Ed. Engl. **33**, 2024 (1994); N. Willenbacher and H. Spiering, J. Phys. C **21**, 1423 (1988); H. Spiering and N. Willenbacher, J. Phys. Condens. Matter **1**, 10089 (1989); M. Nishino, K. Boukheddaden, Y. Konishi, and S. Miyashita, Phys. Rev. Lett. **98**, 247203 (2007).

[8] C. Timm, Phys. Rev. B **73**, 014423 (2006).

[9] S. Sarkar, K. Tarafder, P. M. Oppeneer, and T. Saha- Dasgupta, J. Mater. Chem. **21**, 13832 (2011).

[10] H. Jeschke, L. Salguero, B. Rahaman, C. Buchsbaum, V. Pashchenko, M. U. Schmidt, T. Saha-Dasgupta, and R. Valenti, New J. Phys. **9**, 448 (2007).

[11] T. Bucko, J. Hafner, S. Lebègue, and J. G. Ángyán, Phys. Chem. Chem. Phys. **14**, 5389 (2012).

[12] S.-i. Ohkoshi, K. Imoto, Y. Tsunobuchi, S. Takano, and H. Tokoro, Nat. Chem. **3**, 564 (2011).

[13] G. Kresse and J. Hafner, Phys. Rev. B **47**, 558 (1993); G. Kresse and J. Furthmüller, Phys. Rev. B **54**, 11169 (1996).

[14] P. E. Blöchl, Phys. Rev. B **50**, 17953 (1994); G. Kresse and D. Joubert, *ibid.* **59**, 1758 (1999).

[15] J. P. Perdew, K. Burke, and M. Ernzerhof, Phys. Rev. Lett. **77**, 3865 (1996).

[16] S. L. Dudarev, G. A. Botton, S. Y. Savrasov, C. J. Humphreys, and A. P. Sutton, Phys. Rev. B **57**, 1505 (1998).

[17] S. Lebègue, S. Pillet, and J. G. Ángyán, Phys. Rev. B **78**, 024433 (2008).

[18] See the Supplemental Material http://link.aps.org/supplemental/10.1103/PhysRevLett.109.077203 for the information on computational details, optimized crystal structure data, the pressure induced hysteresis, and temperature evolution of Fe–N bond lengths.

[19] A rotated unit cell was used for the calculations, which contains half the number of atoms as compared to that given in Ref. [12].

[20] B. Gallois, J. A. Real, C. Hauw, and J. Zarembowich, Inorg. Chem. **29**, 1152 (1990).

[21] W. Zhou and T. Yildirim, Phys. Rev. B **74**, 180301(R) (2006); D. F. Bahr, J. A. Reid, W. M. Mook, C. A. Bauer, R. Stumpf, A. J. Skulan, N. R. Moody, B. A. Simmons, M. M. Shindel, and M. D. Allendorf, Phys. Rev. B **76**, 184106 (2007); J. A. Greathouse and M. D. Allendorf, J. Phys. Chem. C **112**, 5795 (2008).

[22] H. Paulsen and A. Trautwein, Top. Curr. Chem. **235**, 197 (2004).